

CONFERENCES AND SYMPOSIA

PACS number: 01.10.Fv

Scientific session of the Division of General Physics and Astronomy of the Russian Academy of Sciences (October 25, 2000)

A scientific session of the Division of General Physics and Astronomy of the Russian Academy of Sciences (RAS) was held on October 25 2000 at the P L Kapitza Institute for Physical Problems, RAS. The following reports were presented in the session:

(1) **Razumova K A** (Nuclear Fusion Institute, Russian Scientific Center 'Kurchatov Institute', Moscow) *Transport barrier formation in a tokamak plasma*;

(2) **Marchenko A V** (General Physics Institute, Russian Academy of Sciences, Moscow) *Model for the formation of ice hummocks in a drifting ice cover*.

Brief presentations of these reports are given below.

PACS numbers: **52.30.–q**, **52.35.–g**, 52.55.Fa
DOI: 10.1070/PU2001v044n03ABEH000912

Transport barrier formation in a tokamak plasma

Razumova K A

It is a well-known fact that for many years research has been conducted worldwide on the problem of building a reactor for controlled fusion, a powerful and safe source of energy. The main avenue of research, which has already led to a technically feasible reactor project, uses plasma that has currents flowing through it and is placed in a toroidal magnetic field. The device became known as a tokamak. Here I will not discuss the technical achievements reached in this area of research, such as, say, plasma temperatures as high as 35 keV and the high coefficient of utilization of the magnetic field pressure. Rather, I will speak on the remarkable properties of hot magnetized plasma, an amorphous substance subject to all imaginable instabilities, which in practice exhibits an order that could be expected only in crystals.

In an ideal situation, a plasma placed in a strong magnetic field will have small transport coefficients since the particles participating in collisions can become shifted only by a distance $\Delta x = \rho_{\mathrm{Lar}}$. Actually, even when placed in a strong magnetic field the plasma remains extremely mobile and is subjected to numerous instabilities, which worsens energy and particle confinement. I will not discuss the kinetic instabilities, but, instead, I will touch on large-scale magnetohydrodynamic (MHD) instabilities, the leading factor in determining the behavior of plasmas.

Uspekhi Fizicheskikh Nauk **171** (3) 329 – 338 (2001)
Translated by O A Glebov; edited by M S Aksent'eva

Since in a tokamak there is a current flowing along the plasma ring, the magnetic lines of force wind around the toroidal axis. The spacing of this winding is given by the quantity

$$q = \frac{B_{\mathrm{t}} r}{B_{\mathrm{p}} R},$$

where B_{t} and B_{p} are the strengths of the toroidal and poloidal magnetic fields, and r and R are the small and large radii of the plasma torus. For some radii, the magnetic line of force can, circling the torus one or more times, close on itself. Such surfaces are called rational and are characterized by a number m corresponding to the number of turns prior to closure. If, in addition, such a line of force has wound itself around the toroidal axis, it can be characterized by the number n of turns around the axis. Thus,

$$q = \frac{B_{\mathrm{t}} r}{B_{\mathrm{p}} R} = \frac{m}{n}.$$

From the standpoint of energy, it is advantageous for the current to flow along a real line of force rather than along the torus, with the result that a plasma with a current is unstable against concentrating along a pencil of rational lines of force. Such a helical current bunch generates its own magnetic field, which forms a 'magnetic island'. The island will grow, but its nonlinear interactions with the rest of the plasma limits this growth, with the result that the island is of finite dimensions. The size of the island depends on the variation of the 'twist' of the magnetic lines of force around the radius of what is known as magnetic shear:

$$S = \frac{r}{q}\,\frac{\mathrm{d}q}{\mathrm{d}r}.$$

The larger the value of S, the smaller the island.

Neighboring islands may adjoin each other along their edges. Nonlinear interaction at the edges leads to granulation of the islands and even to the emergence of regions with damaged magnetic surfaces, i.e. regions where the lines of magnetic force are randomly mixed. Due to the very high transport along the magnetic field, the plasma pressure in the outer and inner parts of the island easily evens out. There is also good thermal contact between islands, with the result that the heat and the particles rapidly leave the area in a direction transverse to the magnetic field.

The list of instabilities in plasma is extremely long. To each action the plasma responds by generating an instability, which changes the plasma's transverse transport path. But each instability, drawing its energy from the unfortunate gradient of a plasma parameter, leads to changes in this gradient and to stabilization. Thus, the plasma tends to

organize its profile in such a way so as to become as stable as possible, i.e. to acquire a configuration with minimum internal energy. One can expect that for different tokamaks and a broad class of tokamak operational regimes the dimensionless plasma pressure profiles are similar, provided that one is able to find the correct normalization for the plasma radius. This is demonstrated by Fig. 1 [1].

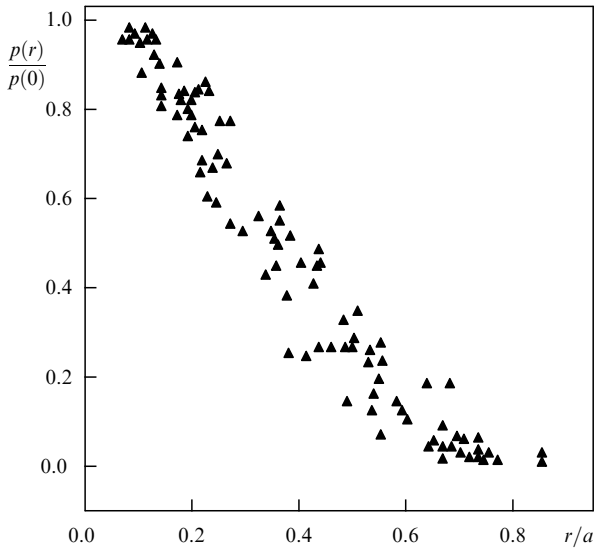

Figure 1. Dependence of the renormalized plasma pressure on the dimensionless radius $\rho = r/a$, where $a = (IR/B_t)^{1/2}$, for different tokamaks and a broad class of operational regimes (T-10, T-11, TFR, TM-3, PLT, PDX, ASDEX).

It was found that the 'current' radius must be normalized to the radius of a magnetic surface with a given q. B B Kadomstev explained this phenomenon and showed that a profile close to a self-consistent one corresponds to the minimum of internal energy [2]. This leads to a situation in which the transport coefficients depend not only on the local characteristics but also on the state of the plasma as a whole.

Naturally, there can be no ideal profile, since the plasma is constantly exposed to various factors. The strongest of these are the boundary conditions, which distort the self-consistent profile and, hence, increase the energy and particle flux to the chamber wall. If we could create a narrow layer with small transport coefficients near the edge of the plasma, the wall would be separated from the plasma and the profile would be closer to the optimal one.

No matter how fantastic this idea sounds, it was actually realized once.

A group of researchers working with the German ASDEX tokamak discovered an operational regime with an external transport barrier (a local minimum of transport coefficients). The electron temperature T_e and electron concentration n_e were found to have steep gradients at the edge of the plasma. This type of regime became known as the H-mode, and in it the plasma confinement is longer by a factor of roughly two. Although empirically the conditions under which such a regime is formed have been thoroughly studied and although this regime has been adopted as the main one for the reactor, the physics of this formation is far from clear. Why, in a narrow zone near a certain magnetic surface, are the conditions for plasma confinement much better?

One of the reasons for this is the formation of rapid poloidal rotation ($V_p \approx 1-5 \times 10^6$ cm s^{-1}) within a small layer of the plasma periphery. The most probable instability responsible for the loss of heat from ions and particles proper is the drift – gradient mode, in which the plasma is ejected in the form of relatively long-wave 'tongues'. Nonuniform rotation along the radius smears these tongues and prevents the development of the instability. Experiments have corroborated this result. But where does the rotation come from? Why does the electron confinement time increase?

Nature prepared another present for the researchers—local internal transport barriers. The theory predicts than many MHD instabilities can be stabilized if $S < 0$, i.e. the current has a hollow profile. Such a configuration emerges either because of a skin-effect or in generation of a non-inductive current in the proper zone of the plasma.

In the beginning the experiments followed the first path. During the current-growth phase the plasma was subjected to powerful additional heating: a flux of high-energy neutral atoms was injected into the plasma at an angle to the magnetic field, and the recharging of these atoms heated the plasma. Improvement of confinement was discovered by Synakowskiĭ et al. [4] (Fig. 2), but the zones with reduced transport coefficients proved to be not in the region where $S < 0$ but in the zero-shear zone. By such heating method torque is introduced into the plasma. This could serve as an explanation of the phenomena, as the presence an external barrier explains the H-mode. However, experiments were soon held in which heating did not introduce a torque into the plasma, while a local transport barrier still appeared.

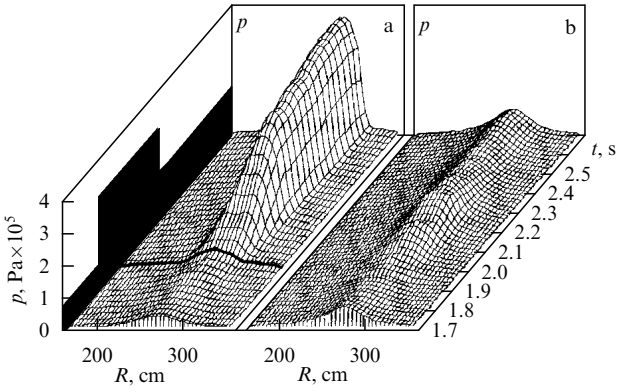

Figure 2. U.S. TFTR facility. Variations in the plasma pressure profile in the process of local transport barrier formation (the left diagram), and an ordinary regime with close initial parameters. The black contour depicts the power fed to the plasma as a function of time. (a) Discharge with a local barrier; (b) discharge without a local barrier.

The T-10 tokamak at the Russian Scientific Center 'Kurchatov Institute' uses electron cyclotron resonance (ECR) as a source of additional heating (naturally, only electrons are heated in this method). If the ECR waves are input at an angle to the magnetic fields, noninductive generation of a current in a given fairly narrow zone of the plasma is possible. Here no torque is introduced into the plasma. The zone of the introduced power and current generation amounts to three-tenths of the total radius of the plasma (such a zone can be made even more local). Thus, current may be generated at different radii both in the direction coinciding with that of the plasma current (CoCD)

and in the opposite direction (CounterCD), which means that the profile $q(r)$ can be changed arbitrarily (Fig. 3).

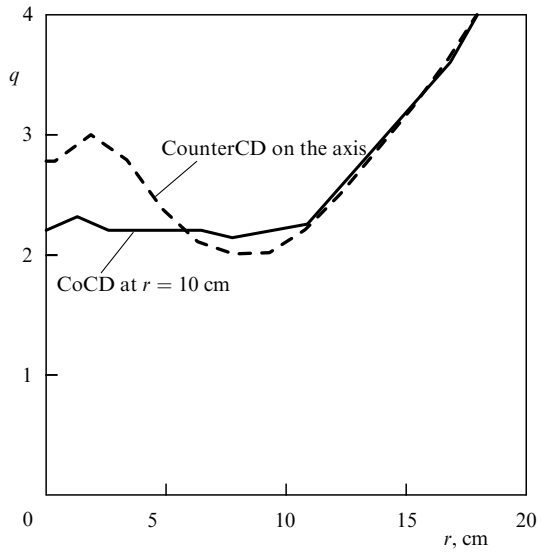

Figure 3. Calculated profiles $q(r)$ for measured profiles $T_e(r)$ and $n_e(r)$ in the generation of CounterCD at the center of the plasma and CoCD at one-third of the plasma radius.

Experiments conducted with T-10 by a group of researchers have shown [5] that local barriers can appear at a negative shear with a central CounterCD or with a noncentral CoCD, with the barrier always forming in the region with low shear and values of q close to the rational one. Since the current is generated not immediately after ECR sets in but gradually increases due to the skin redistribution process, the $q(r)$ profile also changes gradually. When the region $dq/dr = 0$ approaches the rational value, the MHD instability level decreases sharply and a barrier begins to form. A further increase in q_0, which corresponds to the zero derivative, and its passage through the rational value lead to a new upsurge of MHD activity, followed by stabilization near the rational surface and formation of a new barrier (Fig. 4).

If the value of q_0 corresponds to the limit in the condition for barrier formation, the improvement of confinement in the inner zone and the corresponding redistribution of the current density can, as a result of q decreasing within the barrier, force this quantity to leave the necessary range of values, so that the barrier disintegrates. In this case a periodic improvement and deterioration of confinement is observed.

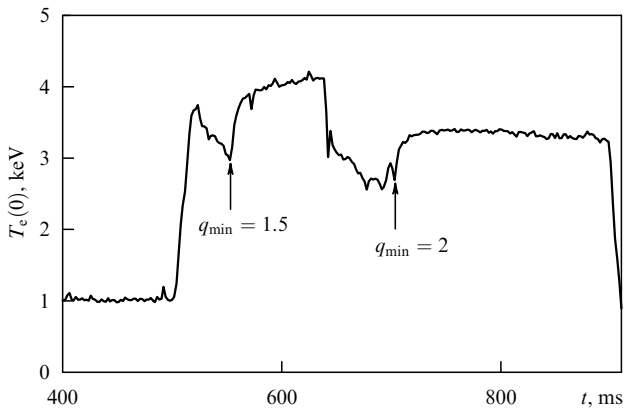

Figure 4. Consecutive emergence of an MHD instability and the formation of local barriers caused by changes in the profile $q(r)$ in the discharge process.

Let us follow the process of barrier formation using the example of the changes in the intensity of X-ray radiation (Fig. 5). What is interesting is that the process begins not only when the electron temperature begins to increase in the ring, where the barrier forms, but also with the simultaneous central region temperature begins to drop, even if the entire ECR power is input at the center (central CounterCD). Only after the barrier has completely formed will the central region of the plasma begin to fill.

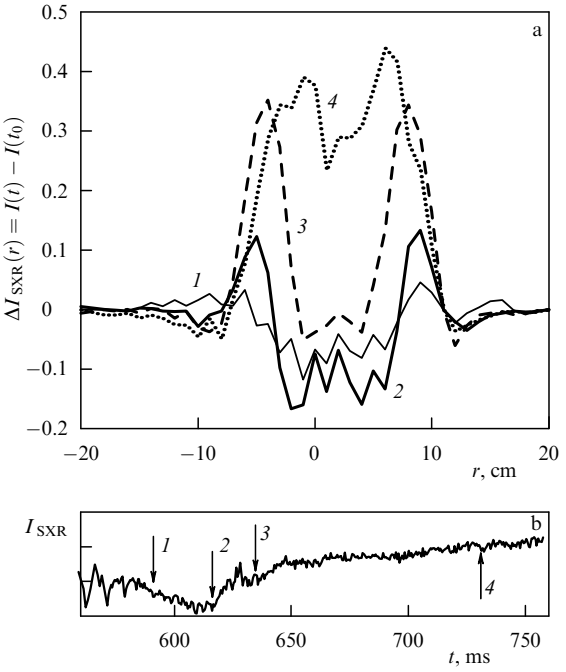

Figure 5. (a) Spatial distribution of the increase in intensity of soft X-ray radiation, I_{SXR}, measured along the chords in the process of barrier formation. The intensity $I(t_0)$ at the moment $t_0 = 570$ ms prior to barrier formation is subtracted from the measured intensity $I(t)$. Restoration of the profile by Abel's method substantially enhances the effect. (b) The arrows indicate the moments in time for which the profiles are given.

Thus, we see that the formation of a local electron transport barrier requires that a certain profile $q(r)$ exist in the vicinity of the resonance surface. And what role does rotation play? We know that it has been shown that namely plasma velocity shear determines the formation of local gradient of particle concentration and ion temperature.

Let us again turn to the experiments conducted on the T-10 tokamak. Here an important result was obtained thanks to the unique methods of plasma diagnostics developed in connection with these experiments, methods that made it possible to measure the changes in the potential profile in the plasma by probing the plasma with beams of heavy ions [6]. When the ECR power was input at one-half of the plasma radius, a barrier at the rational surface $q = 1$ was found to form in this region. Naturally, MHD instabilities, which appeared inside the region, reduced the energy confinement time. Nevertheless, a certain increase in the electron temperature was observed (Fig. 6). The experimenters were able to

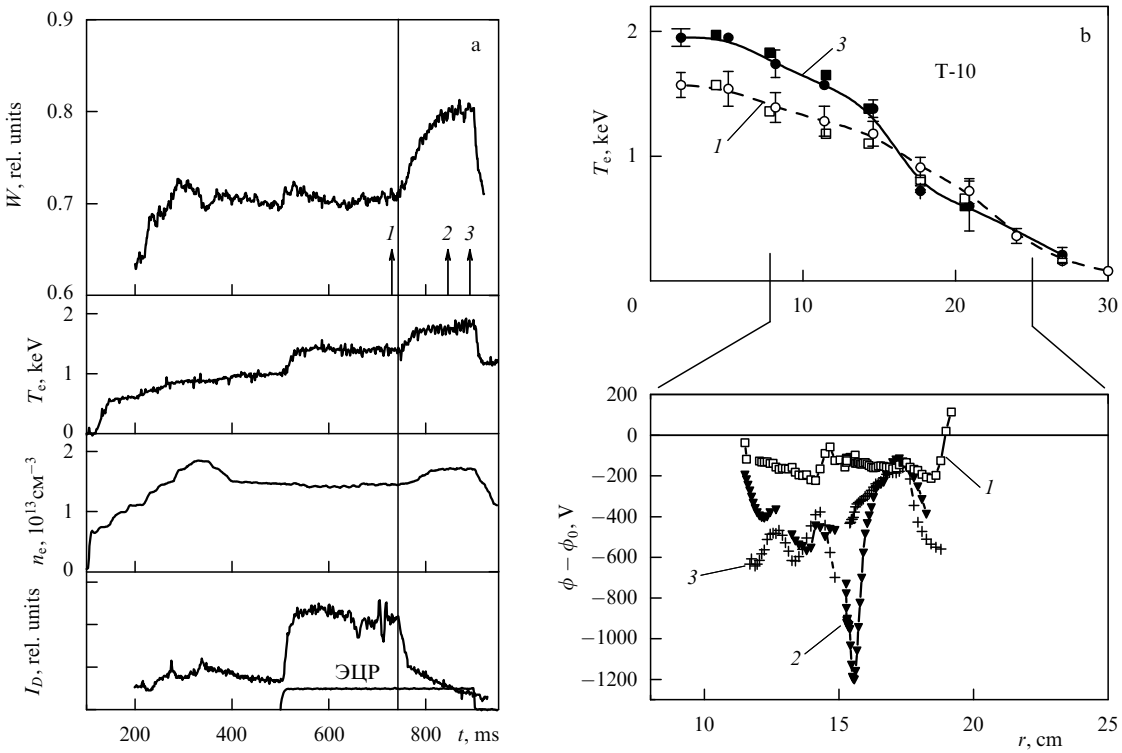

Figure 6. Formation of the local barrier with the ECR power input at one-half the plasma radius. (a) Downward: variation of the plasma energy content (W), variation of T_e inside the barrier ($r = 17$ cm), the plasma concentration as a function of time, and the intensity of the deuterium line characterizing the influx of neutrals to the plasma; the time interval in which ECR is active is indicated in the lower part of this figure. (b) Electron temperature profiles and the variation of plasma potential with time in the process of barrier formation. The moments *1*, *2*, and *3* are as follows: *1*, prior to the formation of the local barrier; *2*, in the process of local barrier formation; and *3*, after formation of the local barrier has been completed.

measure the relative electric potential of the plasma, $\phi - \phi_0$. The measurements showed that a deep narrow potential well formed near the barrier as the temperature T_e increased. This is an indication that near the barrier the balance between the ambipolar fluxes of electrons and ions was disrupted, while the Coulomb forces instantaneously brought the situation into balance again.

What initiated this disbalance? Did the ion flux increase in strength? No, the experiment showed that ion confinement had increased by a factor of 1.5. Hence the electron confinement improved. The new potential well generated a strong electric field that rapidly varied along the radius, with the result that a rotation velocity shear emerged, so that confinement of the ion component improved.

Thus, the process begins with the profile $q(r)$ and the increase in the electron lifetime. What is the relationship here? This question has still to be answered. In the steady-state phase of the process the well is transformed into a steplike decrease of potential toward the inner side of the torus (see Fig. 6).

One more remarkable phenomenon was observed in the experiments involving the T-10 tokamak. The formation of the local barrier is accompanied (simultaneously!) with the formation of an external barrier separated from the former by one-half of the tokamak radius.

The pattern of formation of this external barrier is quite similar to that observed inside — a potential well is formed. However, here particle confinement is improved, and the electron concentration gradient increases. A thorough examination shows that double and even triple barriers are observed in many experiments with different tokamaks. How are these surfaces connected? What a connection do exist between these surfaces? Indeed, there is not a single mode in a torus that can exist in pure form, since the harmonics of this mode are also generated. In the case at hand the local barrier was formed at $q = 1$, while the external barrier was formed at $q = 2$. Possibly, a substantial change in the profile of a magnetic island on one resonance surface may lead to a similar change on another such surface. But then we are forced to believe that the H-mode also begins its formation within a region with a given shear near the resonance surface. The scientific community is not yet ready for such a discovery, and so the question remains open. What is true is that plasma is capable of resounding like a cavity.

Thus, local barriers destroy the bonds in the plasma that (due to turbulence) determined self-consistent profiles and make it possible for steeper parameters gradients to set in local layers. The nonlinearity in the development of instabilities in the high-temperature plasma of a tokamak leads not to chaotization and disintegration of the plasma but to formation of self-organizing structures capable of producing high particle and energy confinement characteristics.

This makes it possible in terrestrial conditions to reach, within limited volumes, plasma temperatures ($T \leqslant 4 \times 10^8$ K) that exceed the temperature inside the Sun by tens of times.

References

1. Esipchuk Yu V, Razumova K A *Plasma Phys. Contr. Nuclear Fusion Res.* **28** 1273 (1986)
2. Kadomtsev B B *Fiz. Plazmy* **13** 771 (1987) [*Sov. J. Plasma Phys.* **13** 443 (1987)]
3. Wagner F et al. *Phys. Rev. Lett.* **49** 1408 (1982)

4. Sinakovski E J et al. *Phys. Plasmas* **4** 1736 (1997)
5. Razumova K A et al. *Plasma Phys. Control. Fusion* **42** 973 (2000)
6. Razumova K A et al., in *27th EPS Conf. on Controlled Fusion and Plasma Phys*. P2039 (2000) p. 205

PACS numbers: 83.10.Dd, 83.80.Nb, 92.10.Rw
DOI: 10.1070/PU2001v044n03ABEH000934

Model for the formation of hummocks in a drifting ice cover

A V Marchenko

1. Introduction

Hummocks constitute a characteristic feature of the sea ice cover. They are produced by the deformations caused by the compression and shearing of the ice cover generated by wind and sea currents. The hummocks are formed in the open ocean and in the vicinity of the shores and greatly affect navigation in the ice-covered sea of the Arctic regions. The hummocks produced in the sea-shelf regions near the hydrotechnical structures greatly affect the distribution of the loads exerted by the ice on these structures.

The hummocks are pieces of ice pushed out under and over the surface of the surrounding flat ice cover. The above-water part of a hummock, the sail, may be several meters high while the height of the underwater part, the keel, may be tens of meters. Hummocks are fairly often extended horizontally [1]. Hummocks have a significant influence on the rheological properties of the ice cover and make it spatially inhomogeneous and anisotropic.

Theoretical modeling of hummock formation (the ridging process) may be classified into two types of analyses. In the studies of the first type (see, for instance, [2]) the ridging processes are taken into account in the large-scale simulation of the ice cover dynamics. Ridging is treated as the main mechanism for evolution of the ice cover thickness profile. The simulation yields the evolution of the thickness distribution for the ice cover under plastic strain. The structure and evolution of an individual hummock are ignored in the simulation process.

The first model of hummock formation was developed by Parmeter and Coon [3] in 1973. Parmerter and Coon analyzed the observational data and put forward a hypothesis that there was a maximum hummock height depending on the thickness of the ice sheets making up the hummock. According to the hypothesis, a hummock grows in height and width if its vertical dimension is smaller than the maximum size and after its height has reached the maximum size only the hummock width grows. The maximum hummock height is determined by the bending load breaking down the edge of the floe pushing against the hummock owing to the lack of balance between gravity and the lifting force acting on the hummock edge in water. Parmeter and Coon estimated the compression stress required for the hummock formation from the equations for conservation of mass and energy.

Hopkins and co-workers [4, 5] used a different approach to modeling the ridging process. They treated a hummock as a pile of ice blocks of a given shape with viscous elastic forces acting between them. The motion of each ice block is described by a separate equation. New ice blocks are produced in the model when the floe edge pushes against the hummock. High-capacity computer simulations involved calculations of the motion for the large number of ice blocks making up the hummock yielding a realistic representation of the ridging process and confirming the hypothesis of the maximum hummock height.

It was only in 1998 that a hummock was produced under laboratory conditions [6] in the ice basin of the Technological University in Helsinki. The thickness of the artificially frozen ice was not more than 10 cm. The experimental results demonstrated that the growth of the hummocks under compression was accompanied by floes being pushed under hummocks so that these two processes cannot be monitored separately in practice. The results of the laboratory experiments are corroborated by the data of observations conducted in northern Baltic Sea which demonstrated that ice hummocks were largely composed of flat floes piled up on each other.

The objective of the present study was to develop a model of the ridging process that would make it possible to analyze the formation of hummocks in the ice cover consisting of an arbitrary number of floes. It is assumed that the hummocks are formed at the lines of contact between floes driven by winds. The suggested mechanism is valid for the sea ice cover in which the regions of flat and ridged ice can always be identified. A flat ice cover region is broken down under compression so that hummocks are produced while the flat ice regions are displaced with respect to each other. It will be demonstrated that the displacements are periodic owing to the self-sustained oscillations accompanying shifting of the drifting ice [7].

2. Basic equations

Let us consider the conservation of mass, momentum, and energy for an ice layer floating on a liquid surface. The appropriate differential equations for the one-dimensional case are

$$\frac{\partial m}{\partial t}+\frac{\partial mv}{\partial x}=0\,,$$
$$\frac{\partial mv}{\partial t}+\frac{\partial mv^2}{\partial x}=\frac{\partial \sigma}{\partial x}+f,$$
$$\frac{\partial E}{\partial t}+\frac{\partial Ev}{\partial x}=\frac{\partial \sigma v}{\partial x}+fv\,. \qquad (2.1)$$

Here m is the mass of the ice floating on the unit surface area of the ocean, v is the ice drift velocity, σ are the internal stresses in the ice, E is the surface energy density of the ice, f is the friction force of the atmosphere and the ocean acting on the ice, x is the horizontal coordinate, and t is the time.

The ice concentration on the ocean surface is assumed to be unity and we can write $m=\rho_{\rm i}h(x,t)$ where $h(x,t)$ is the ice thickness and $\rho_{\rm i}\approx 930$ kg m^{-3} is the sea ice density. The surface energy density of the ice cover is given by the equation

$$E=K+P+W, \qquad (2.2)$$

where $K=\rho_{\rm i}hv^2/2$ is the surface density of the kinetic energy, and P and W are the surface densities of the potential and internal energies.

The surface density of the potential energy of the floating ice is given by the equation

$$P=\rho_{\rm i}g\int_{z_-}^{z_+} z\,{\rm d}z-\rho_{\rm w}g\int_{z_-}^{0} z\,{\rm d}z \qquad (2.3)$$

It equals the difference between the potential energy of the ice taken from the level $z = 0$ of the unperturbed liquid surface and the potential energy of the liquid displaced by the ice. Here $\rho_w \approx 1020$ kg m^{-3} is the seawater density. The upper and lower surfaces of the ice cover are determined by the equations $z = z_-(x, t)$ and $z = z_+(x, t)$. The thickness of the ice cover is $h = z_+ - z_-$.

A further simulation step included the processes of irreversible ice cover compression accompanied with variation of its thickness and dissipation of the mechanical energy. The variation of the internal energy is determined by the energy dissipation

$$\mathrm{d}W = \mathrm{d}D \geqslant 0\,. \tag{2.4}$$

The variation of the ice thickness under compression is determined by ridging and rafting processes. Ridging gives rise to hummocks produced by ice rubble. Rafting is the piling up of flat ice sheets. Sometimes compression is determined by a combination of ridging and rafting.

As the ice thickness grows the potential energy of the ice increases irreversibly,

$$\mathrm{d}P \geqslant 0\,. \tag{2.5}$$

Let us assume that a flat ice cover includes a ridged ice region with the boundaries $x = x_-(t)$ and $x = x_+(t)$. For $x < x_-$ and $x > x_+$ the ice thickness is constant and equals $x = x_-$ and $x = x_+$, respectively.

$$\frac{\mathrm{d}U_r}{\mathrm{d}t} = [hQ]\,, \tag{2.6}$$

$$\frac{\mathrm{d}I_r}{\mathrm{d}t} = [\sigma] + \rho_i[hvQ] + F_r\,, \tag{2.7}$$

$$\frac{\mathrm{d}E_r}{\mathrm{d}t} = [\sigma v] + [EQ] + A_r\,, \tag{2.8}$$

where U_r, I_r and E_r are the linear density of volume, impulse and energy of the ice in the region $x \in (x_-, x_+)$, and $[\lambda] = \lambda_+ - \lambda_-$ for any symbol λ or combination of symbols

The flows $Q_+ \geqslant 0$ and $Q_- \leqslant 0$ are defined by the formulae

$$Q_\pm = \frac{\mathrm{d}x_\pm}{\mathrm{d}t} - v_\pm\,, \tag{2.9}$$

where v_+ and v_- are the ice drift velocities in the regions $x > x_+$ and $x < x_-$.

The values σ_+ and σ_- are equal to the stress in the flat ice covers for $x = x_+$ and $x = x_-$; E_+ and E_- are the ice surface energy densities in the region $x > x_+$ and $x < x_-$, F_r is the external drag force, acting on the ridge by $x \in (x_-, x_+)$, and A_r is the power of this force.

The system of equations (2.6)–(2.8) is a generalization of the relationships at a discontinuity [8] for the case when material is built up at the fracture. Similar relationships have been considered in the theory of gas diffusion with an admixture of dispersive particles [9], where the necessity of their inclusion was connected with the overturning of compression waves. Such a surface has been called 'sheet'. Physically, the sheeting corresponds to those regions where one may not neglect the collisions between particles of the admixture. Sheet fractures have been used to describe the formation and drift of bands of unbroken ice in a dispersive ice cover [10, 11]. In this case, the properties of the material also change on the surface of the fracture since the ice cover inside the hummock is made up of lumps of ice.

3. Evaluation of the characteristic scale of the problem

The friction force acting between the ice cover and the water determines a rather low velocity of ice drift under natural conditions. Therefore, we can take $V = 0.1$ m s^{-1} as a characteristic scale of the ice drift velocity [12].

In the conditions under consideration the characteristic time scale for the ice drift is determined by the self-sustained oscillations of the ice cover. The observational data demonstrate that for a constant wind acting on the ice, the ice deformation proceeds in the form of quasi-periodic shifts produced by the relative displacements of the floes [7]. The period of such shifts can be as long as several minutes [13]. This is why $T = 1$ min is selected as a characteristic time scale.

The measurements made under natural conditions for the ice cover [14] yielded the highest stresses of the order of 10^5 N m^{-1}. Stresses of the order of 10^4 N m^{-1} correspond to the initial stages of the ridging process. This is why we have selected $\Sigma = 10^4$ N m^{-1} as a characteristic stress.

Let us make an order-of-magnitude estimate of the terms in equations (2.6)–(2.8). The friction force with which the water is acting on the hummock keel is estimated as

$$F_r = \rho_w C_w h_k \delta v^2\,,$$

where $C_w \approx 1$ is the resistance coefficient for non-streamlined bodies, δv is the difference between the velocities of the water and the ice, and h_k is the distance from the point of the hummock which is the deepest in the water to the lower ice surface. For the sake of assessments we shall take $h_k \approx 10$ m and $\delta v \approx 0.1$ m s^{-1}. Then the assessment yields $F_r \approx 100$ N m^{-1}.

Let us evaluate the inertial term in equation (2.7) assuming that the hummock has a triangular sail shape with side edge angles of the sail and keel being 30° (see Fig. 1) [1]. Under such conditions the hummock volume per unit length is $U_r \approx 2h_k^2 = 200\,\mathrm{m}^2$. The inertial term is of the order of $\rho_i U_r V T^{-1} \approx 300$ N m^{-1}.

Let the characteristic ice thickness be $h = 1$ m. The penultimate term on the right-hand side of equation (2.7) is of the order of $\rho_i h V^2 \approx 10$ N m^{-1}. Hence we obtain the estimate $[\sigma] \ll \Sigma$. In other words, the difference between stresses on two sides of a triangular hummock is much smaller than the stresses themselves. Therefore, we can take

$$[\sigma] = 0\,. \tag{3.1}$$

in the stress calculations. Note that this equation is inapplicable to hummocks of trapezoid shape with a fairly large

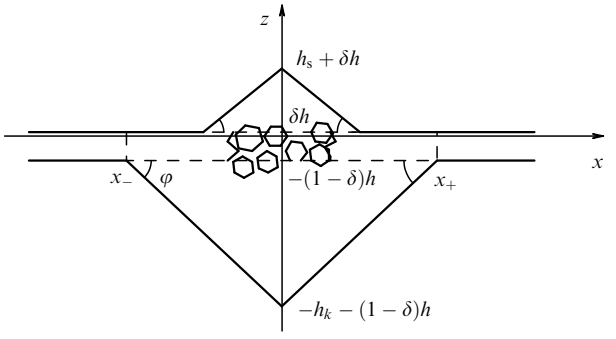

Figure 1.

volume U_r. Let us estimate the width of a trapezoid-shaped hummock for which the inertial term is of the order of $10^5 \mathrm{N\,m^{-1}}$ (the extreme stresses generated with the formation of large hummocks). Let us take $U_r \approx (h_k + h_s)L_r$ where h_s is the sail height and $h_k + h_s = 20$ m. The condition $\rho_i U_r V T^{-1} \approx 10^4 \mathrm{\ N\,m^{-1}}$ yields $L_r \approx 300$ m.

Using similar estimates we can demonstrate that in equation (2.8) for the energy the characteristic values of both the kinetic energy of the hummock and the work A_r are much smaller than other terms of the equation. Therefore, we shall assume below that

$$\mathrm{d}E_r = \mathrm{d}P_r + \mathrm{d}D_r\,. \tag{3.2}$$

Let us estimate the characteristic values of the densities of the potential P_f and kinetic K_f energies of a flat ice cover. These densities are given by

$$2P_f = \delta\rho_i g h^2\,, \quad 2K_f = \rho_i h v^2\,, \tag{3.3}$$

where v is the drift velocity and h is the ice thickness. Assuming $v \approx V$ and $h \approx 1$ m we obtain $K_f \ll P_f$. Using this estimate we assume below that

$$E_f = P_f\,. \tag{3.4}$$

4. Hypotheses on the self-similarity of the hummock shape and energy dissipation

The hypothesis that the hummock shape is self-similar consists in the assumption that the variation of the shapes of the underwater and above-water parts of the hummock (the sail and the keel) is determined by the variation of the hummock volume during the ridging process. The sail and the keel of the hummock are at hydrostatic equilibrium in the course of the process. Hence we obtain the equations

$$\mathrm{d}P_r = \frac{\mathrm{d}P_r}{\mathrm{d}U_r}\,\mathrm{d}U_r\,, \quad \mathrm{d}L_r = \frac{\mathrm{d}L_r}{\mathrm{d}U_r}\,\mathrm{d}U_r\,, \tag{4.1}$$

where $L_r = x_+ - x_-$ is the hummock width.

The observational data indicate that the shape of the hummock sail and keel are often close to a triangular or trapezoid shape [1]. For a hummock of triangular shape with the same angle φ of the side edges of the sail and the keel produced in a flat ice cover of the height h (see Fig. 1) the self-similarity hypothesis yields the following equations

$$\begin{aligned} &U_r = hL_r + AL_r^2\,,\\ &2P_r = \rho_i g L_r\left[\delta h^2 + 2L_r(\delta A h + BL_r)\right],\\ &2h_k = L_r \operatorname{tg}\varphi\,, \quad h_s = \gamma h_k\,, \end{aligned} \tag{4.2}$$

where the coefficients A, B, and γ are given by the equations

$$\begin{aligned} &4A = (1 + 2\gamma^2)\operatorname{tg}\varphi\,,\\ &24B = (1 + 2\gamma)(\gamma \operatorname{tg}\varphi)^2\,,\\ &\gamma = \sqrt{\frac{\delta}{1-\delta}}\,, \quad \delta = \frac{\rho_w - \rho_i}{\rho_w}\,. \end{aligned}$$

The self-similarity hypothesis is satisfied in the process of rafting of two floes (see Fig. 2). Under these conditions the following equations are satisfied:

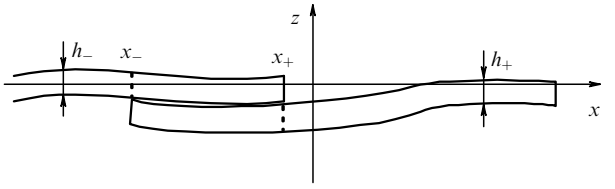

Figure 2.

$$U_r = L_r(h_+ + h_-)\,, \quad 2P_r = \rho_i \delta g L_r (h_+ + h_-)^2\,. \tag{4.3}$$

To determine the dissipative function we shall take

$$\mathrm{d}D_r = (\sigma_d^+ Q_+ - \sigma_d^- Q_-)\,\mathrm{d}t \geqslant 0\,, \tag{4.4}$$

in accordance with the general principles of thermodynamics. Here $\sigma_d^\pm$ are the generalized thermodynamic forces which are determined by the scenario of the ridging process.

The following scenario of the ridging process is quite well-known [1]. The ice cover from the region with $x > x_+$ pushes against the right-hand edge side of the hummock sail. In the process the flat ice sheet is broken into pieces of rubble which fall on both sides of the sail. The edge of the ice sheet pushing into the hummock from the region with $x < x_-$ is broken under the weight of the hummock sail. The hummock keel is formed of the ice rubble pushed down into the water by the weight of the hummock sail.

The energy dissipation is determined primarily by the friction of the ice sheet slipping over the hummock sail on the right-hand side of the hummock sail. It is assumed, therefore, that $\sigma_d^- = 0$ while σ_d^+ is given by the law of dry friction according to the equation

$$\sigma_d^+ = \mu\rho_i g h h_s \operatorname{ctg}\varphi\,, \tag{4.5}$$

where μ is the friction coefficient. According to equations (4.2), the generalized force σ_d^+ is a function of the hummock volume.

In the process of rafting the mechanical energy is dissipated by means of friction between the ice floes. Assume that the ice sheet from the region with $x > x_+$ is under the ice sheet from the region with $x > x_-$ (see Fig. 2). Assuming that the interaction between the ice sheets is described by the law of dry friction we obtain the equation

$$\mathrm{d}D_r = \mu\rho_i g h_- L_r\,\mathrm{d}L_r\,, \tag{4.6}$$

where μ is the friction coefficient.

Equations (4.4) and (4.6) yield

$$\sigma_d^\pm = \mu\rho_i g h^- x^\pm\,. \tag{4.7}$$

Equations (4.4) imply that $\mathrm{d}D_r$ is a function of the volume variation $\mathrm{d}U_r$.

5. Ridging stress

Let us analyze several simple mathematical models of ridging in which the stresses required for the ice ridging process are found from the system of equations (2.6)–(2.8) as functions of the hummock volume and the thickness of the ice making up the hummock.

5.1 Rafting

It can be readily seen that the following equations are satisfied in the rafting process:

$$\frac{\mathrm{d}x_{\mp}}{\mathrm{d}t} = v_{\pm}\,, \quad Q_{+} = -Q_{-} = -[v]\,. \tag{5.1}$$

The volume and the potential energy of the ice in the rafting region are given by equations (4.3). Equation (4.6) determines the dissipation of the mechanical energy. Using equations (3.1), (3.2), (3.4), and (5.1) we can rewrite equations (2.6) and (2.8) as

$$\frac{\mathrm{d}U_{\mathrm{r}}}{\mathrm{d}t} = -(h_{+} + h_{-})[v]\,, \tag{5.2}$$

$$\frac{\mathrm{d}P_{\mathrm{r}}}{\mathrm{d}t} + \frac{\mathrm{d}D_{\mathrm{r}}}{\mathrm{d}t} = \sigma_{\mathrm{r}}[v] - (P_{\mathrm{f}}^{+} + P_{\mathrm{f}}^{-})[v]\,.$$

Hence we obtain the following expression for the stress $\sigma_{\mathrm{r}} = \sigma_{+} = -\sigma_{-}$:

$$\sigma_{\mathrm{r}} = -(h_{+} + h_{-})\left(\frac{\mathrm{d}P_{\mathrm{r}}}{\mathrm{d}U_{\mathrm{r}}} + \frac{\mathrm{d}D_{\mathrm{r}}}{\mathrm{d}U_{\mathrm{r}}}\right) + P_{\mathrm{f}}^{+} + P_{\mathrm{f}}^{-}\,. \tag{5.3}$$

5.2 Ice ridging at a stationary wall

Assume that the ridge is at $x = 0$. The left-hand side of the hummock coincides with the wall while the right-hand side is at $x = x_{+}$. As the hummock shape is self-similar we obtain

$$\mathrm{d}x_{+} = \frac{\mathrm{d}x_{+}}{\mathrm{d}U_{\mathrm{r}}}\,\mathrm{d}U_{\mathrm{r}}\,. \tag{5.4}$$

As $Q_{-} = 0$ we can rewrite equations (2.6) and (2.8) in the following form:

$$\frac{\mathrm{d}U_{\mathrm{r}}}{\mathrm{d}t} = h\left(\frac{\mathrm{d}x_{+}}{\mathrm{d}t} - v_{+}\right), \tag{5.5}$$

$$\frac{\mathrm{d}P_{\mathrm{r}}}{\mathrm{d}U_{\mathrm{r}}}\,\frac{\mathrm{d}U_{\mathrm{r}}}{\mathrm{d}t} + (\sigma_{\mathrm{d}}^{+} - P_{\mathrm{f}}^{+})\left(\frac{\mathrm{d}x_{+}}{\mathrm{d}t} - v_{+}\right) = \sigma_{+}v_{+}\,.$$

Equations (5.4) and (5.5) yield the stress σ_{r} required for ice ridging at the wall:

$$\sigma_{+} = -\left(h\frac{\mathrm{d}P_{\mathrm{r}}}{\mathrm{d}U_{\mathrm{r}}} + \sigma_{\mathrm{d}}^{+} - P_{\mathrm{f}}^{+}\right)\left(1 - h\frac{\mathrm{d}x_{+}}{\mathrm{d}U_{\mathrm{r}}}\right)^{-1}. \tag{5.6}$$

The friction stress σ_{d}^{+} is a function of the hummock volume with the thickness h equal to the flat ice sheet thickness and depends on the scenario of hummock development. If a hummock is triangular in shape then the stress σ_{d}^{+} is given by equation (4.5).

5.3 Development of a triangular hummock in the uniform ice cover

Assume that the ice cover has the same properties on both sides of the hummock and that $h_{+} = h_{-} = h$. Under these circumstances we can assume that the flows of ice into the hummock are identical at both sides:

$$Q_{+} = -Q_{-} = Q\,. \tag{5.7}$$

According to equation (5.7), the midpoint of the hummock moves at the mean velocity of the ice floes making up the hummock and we have

$$2Q = \frac{\mathrm{d}L_{\mathrm{r}}}{\mathrm{d}t} - [v]\,. \tag{5.8}$$

Using equation (5.7) we can rewrite equations (2.6) and (2.8) as

$$\frac{\mathrm{d}U_{\mathrm{r}}}{\mathrm{d}t} = 2hQ\,, \tag{5.9}$$

$$\frac{\mathrm{d}P_{\mathrm{r}}}{\mathrm{d}U_{\mathrm{r}}}\,\frac{\mathrm{d}U_{\mathrm{r}}}{\mathrm{d}t} + (\sigma_{\mathrm{d}}^{+} + \sigma_{\mathrm{d}}^{-} - 2P_{\mathrm{f}})\,Q = \sigma_{\mathrm{r}}[v]\,.$$

Using equation (5.8) we can find the ridging stress

$$\sigma_{\mathrm{r}} = -\left(h\frac{\mathrm{d}P_{\mathrm{r}}}{\mathrm{d}U_{\mathrm{r}}} + \frac{\sigma_{\mathrm{d}}^{+} + \sigma_{\mathrm{d}}^{-}}{2} - P_{\mathrm{f}}\right)\left(1 - h\frac{\mathrm{d}L_{\mathrm{r}}}{\mathrm{d}U_{\mathrm{r}}}\right)^{-1}. \tag{5.10}$$

If the ridging process proceeds via the scenario described in Section 4 then the stress $\sigma_{\mathrm{d}}^{-} = 0$ and σ_{d}^{+} is given by equation (4.5).

6. Self-sustained oscillations of the ice cover caused by ridging

Let us consider the development of triangular hummocks at the boundaries between three ice floes under the effect of wind-generated stresses. The wind velocity is directed towards the sea shore. The hummocks and ice floes are numbered as shown in Fig. 3. floe *3* is stopped by the shore and, therefore, is stationary. The drift velocities for floes *1* and *2* are v_1 and v_2. At the initial moment small hummocks are assumed to exist between the ice floes.

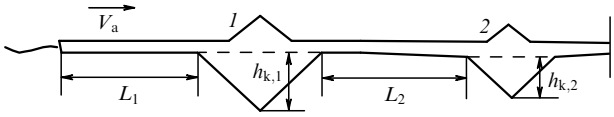

Figure 3.

The complete system of equations describing the process under consideration is

$$\frac{\mathrm{d}L_1}{\mathrm{d}t} = -Q_1\,, \quad \frac{\mathrm{d}L_2}{\mathrm{d}t} = -Q_1 - Q_2\,, \tag{6.1}$$

$$\rho_{\mathrm{i}}\,hL_1\,\frac{\mathrm{d}v_1}{\mathrm{d}t} = f_1 + \sigma_{\mathrm{r},1}(U_{\mathrm{r},1})\,, \tag{6.2}$$

$$\rho_{\mathrm{i}}\,hL_2\,\frac{\mathrm{d}v_2}{\mathrm{d}t} = f_2 - \sigma_{\mathrm{r},1}(U_{\mathrm{r},1}) + \sigma_{\mathrm{r},2}(U_{\mathrm{r},2})\,, \tag{6.3}$$

$$\frac{\mathrm{d}U_{\mathrm{r},1}}{\mathrm{d}t} = 2hQ_1\,, \quad \frac{\mathrm{d}U_{\mathrm{r},2}}{\mathrm{d}t} = 2hQ_2\,. \tag{6.4}$$

Equations (6.1) describe the variation of the ice flow size with the consumption of ice for building up the hummocks. According to the definitions (5.8), the flows Q_1 and Q_2 are given by

$$2Q_1 = \frac{\mathrm{d}L_{\mathrm{r},1}}{\mathrm{d}U_{\mathrm{r},1}}\,\frac{\mathrm{d}U_{\mathrm{r},1}}{\mathrm{d}t} - v_2 + v_1\,,$$

$$2Q_2 = \frac{\mathrm{d}L_{\mathrm{r},2}}{\mathrm{d}U_{\mathrm{r},2}}\,\frac{\mathrm{d}U_{\mathrm{r},2}}{\mathrm{d}t} + v_2\,. \tag{6.5}$$

Equations (6.2) and (6.3) describe the momentum balance for the ice floes *1* and *2*. Equation (5.10) determines the ridging stresses $\sigma_{r,1}(U_{r,1})$ and $\sigma_{r,2}(U_{r,2})$ as functions of the hummock volumes $U_{r,1}$ and $U_{r,2}$. The stresses generated by the friction of wind and water at the surfaces of floes *1* and *2* are denoted as f_1 and f_2 and given by

$$f_{1,2} = (\rho_a C_a V_a^2 - \rho_w C_w v_{1,2}^2) L_{1,2}\,, \qquad (6.6)$$

where ρ_a is the air density, C_a and C_w are the respective friction coefficients, and V_a is the wind velocity.

Equations (5.9) for the ice mass balance yield equations (6.4). The system of six equations (6.1)–(6.4) includes six unknown functions of time L_1, L_2, $U_{r,1}$, $U_{r,2}$, v_1, and v_2 and is closed. Equations (4.2) relate the hummock volumes $U_{r,1}$ and $U_{r,2}$ to the sail heights $h_{s,1}$ and $h_{s,2}$ and the keel drafts $h_{k,1}$ and $h_{k,2}$.

In numerical simulations we assumed that $h = 1$ m, $V_a = 15$ m s^{-1}, $C_a = 0.003$ (see [15]), $C_w = 0.005$ (see [16]), and $\mu = 0.3$ (see [17]). At the initial moment $t = 0$ we took $L_1(0) = 20$ km, $h_{k,1}(0) = 0.5$ m, $h_{k,2}(0) = 0.1$ m, $v_1(0) = 0.3$ m s^{-1}, $v_2(0) = 0$. Figure 4 presents the numerical simulation results for $L_2(0) = 500$ m (a, b), $L_2(0) = 1$ km (c, d), and $L_2(0) = 3$ km (e, f).

The initial conditions indicate that the hummock size is small at the initial moment. The small hummocks can withstand low compression stresses. This is why in the model under consideration they are regarded simply as the zones where the ice cover is weakened and where ridging occurs.

It can be seen that the ridging process goes on for approximately 1.3 hours. In this period the hummock keels grow to approximately 13 m. The hummock sail size is close to 4 m. The final dimensions of the hummock produced on the right-hand side of ice floe *2* are somewhat larger than the dimensions of the left-hand hummock. The motion of the large floe *1* is practically monotonic. The motion of floe *2* exhibits oscillations whose period depends on the floe size. The oscillation periods are approximately 5, 10, and 20 min for $L_2(0) = 500$ m, $L_2(0) = 1$ km, and $L_2(0) = 3$ km, respectively. These oscillations can be regarded as self-sustained oscillations as they are generated only under a steady-state wind load and are determined only by the internal structure of the ice cover which depends on the dimensions of the floes and hummocks. The period of the self-sustained oscillations decreases as the floe size diminishes.

The self-sustained oscillations are generated owing to the non-uniform dissipation of the mechanical energy at the floe edges which is caused by the process of ridging. If at the initial moment both hummocks have identical dimensions, the motion of ice floe *2* does not exhibit oscillations. At the moment when the ridging process is discontinued the hummocks have similar dimensions irrespective of their original sizes.

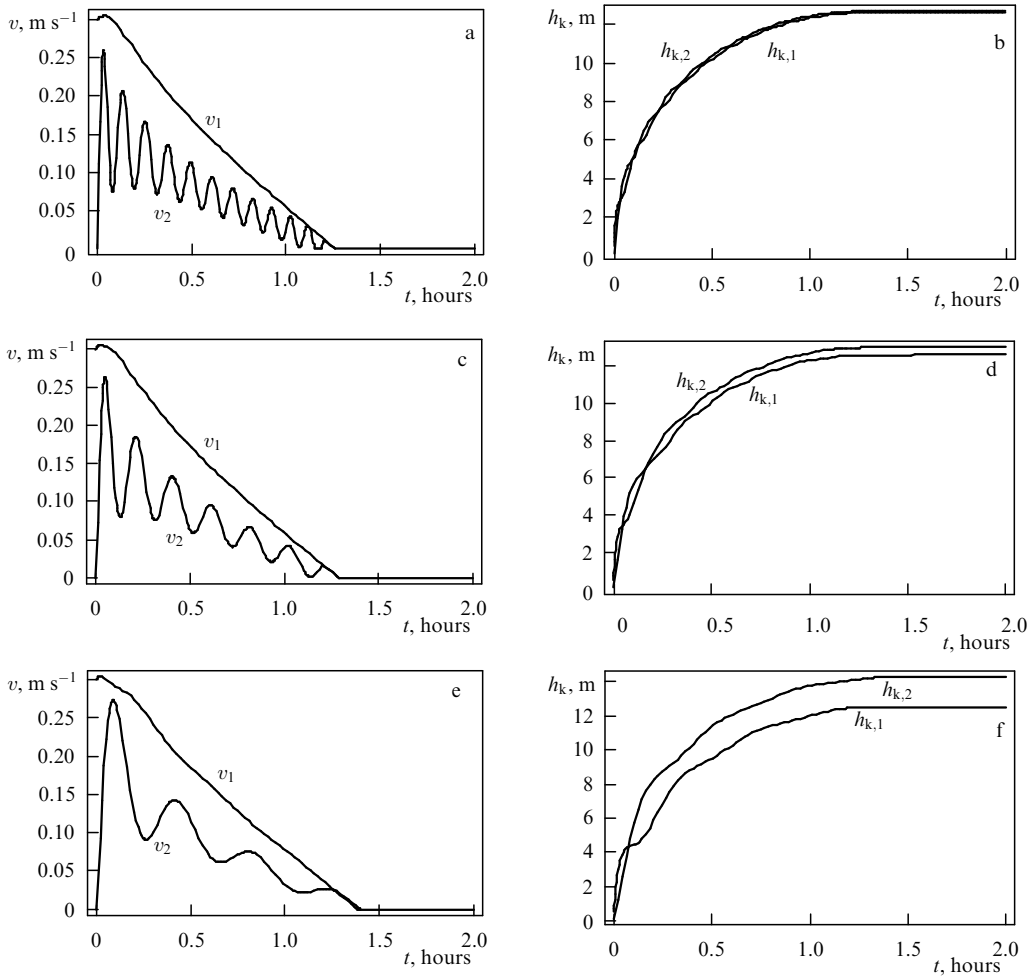

Figure 4.

7. Conclusion

The paper presents a new approach to the modeling of the ridging process in a drifting ice cover based on the representation of a hummock by a discontinuity line in the equations of the ice cover dynamics. The conservation of mass, momentum, and energy yield the relations at the discontinuity line. The stresses required for hummock formation can be calculated from the relations at the discontinuity line as functions of the hummock volume if the hypotheses on the self-similarity of the hummock shape and the energy dissipation are satisfied.

The modeling approach was implemented for the case of flat ice cover when the discontinuity line was straight and the velocities of the floes making up the hummock were perpendicular to the discontinuity line. Equations have been derived for the stresses generated in the process of rafting, in the case of hummock formation at a solid wall, and in the case of compression of a uniform ice cover.

Numerical simulations were conducted for the case of two hummocks formed at the line of contact of three floes of identical thickness and different lengths. The left-hand side of the left-hand floe was assumed to be free, the right-hand floe was stationary and the length of the middle floe was smaller than the length of the left-hand floe. The wind acting on the ice surface causes compression of the ice cover. The computer simulation results demonstrate that after the termination of the ridging process both hummocks have approximately identical dimensions. During the ridging process the velocity of the middle floe exhibits oscillations determined by nonuniform dissipation of the mechanical energy in the hummocks. The oscillation period decreases with a decrease in the length of the middle floe. The calculated period varied from 5 min to 20 min. Observations of drifting ice cover under natural conditions exhibited self-sustained oscillations with such periods [7].

The equations derived for the ridging stresses can be used for developing large-scale rheological ice cover models for appropriate climatic conditions in which the ice cover is treated as a continuous medium with plastic properties. The ridging stresses determine the limiting compression stresses describing the plastic properties of the ice cover.

It is important to calculate the frequencies of the oscillatory motion of the ice cover accompanying ridging near the hydrotechnical structures as they should be known for assessing the effects of ice dynamics on these structures. In particular, it would be useful to analyze a possible resonance between the ice oscillations and the natural frequencies of the structures. Any resonance will enhance the danger of a catastrophic failure of the structure.

The study was supported by the Russian Fund for Fundamental Research (projects 99-01-01150 and 99-02-17005) and by the Norwegian Science Consulate (project 128087/730).

References

1. Kovacs A, Sodhi S *Cold Region Technol.* (2) 209 (1980)
2. Pritchard R, in *Ice in Surface Waters* (Ed. H T Shen) (Rotterdam: Balkema, 1999) p. 1041
3. Parmerter R R, Coon M D *J. Geophys. Res.* **77** 6565 (1972)
4. Hopkins M A *J. Geophys. Res.* **103** (C10) 21883 (1998)
5. Hopkins M A, Tuhkuri J, Lensu M *J. Geophys. Res.* **104** (C6) 13605 (1999)
6. Tuhkuri J, Lensu M, Saarinen S "Laboratory and field studies of ice ridge formation", in *Proc. of the 15th Int. Conf. on Port and Ocean Eng. under Arctic Conditions* (*POAC'99*) Vol. 3 (Helsinki: HUT, 1999) p. 1118
7. Smirnov V N *Dinamicheskie Protsessy v Morskikh L'dakh* (Dynamical Processes in Sea Ice) (St. Petersburg: Gidrometeoizdat, 1996)
8. Sedov L I *Mekhanika Sploshnoĭ Sredy* (Mechanics of a Continuous Medium) Vol. 1 (Moscow: Nauka, 1983) [Translated into English: *A Course in Continuum Mechanics* (Groningen: Wolters-Noordhoff, 1971)]
9. Kraĭko A N *Prikl. Mat. Mekh.* **43** 500 (1979)
10. Marchenko A V *Prikl. Mat. Mekh.* **56** 419 (1992)
11. Makshtas A P, Marchenko A V, in *Zakonomernosti Krupnomasshtabnykh Protsessov v Norvezhskoĭ Energoaktivnoĭ Zone i Prilegayushchikh Raĭonov* (Large-Scale Processes in the Norwegian Energy-Active Zone and Adjacent Regions) (St. Petersburg: Gidrometeoizdat, 1994) p. 150
12. Appel' I L, Gudkovich Z N *Chislennoe Modelirovanie i Prognoz Evolyutsii Ledyanogo Pokrova Arkticheskikh Moreĭ v Period Tayaniya* (Numerical Simulation and Prediction of Ice Cover Evolution during the Melting Period in the Arctic Seas), (St. Petersburg: Gidrometeoizdat, 1992) p. 144
13. Martin S, Drucker R *J. Geophys. Res.* **96** (C6) 10567 (1991)
14. Coon M D, Echert D C, Knoke G S, in *Ice in Surface Waters* (Ed. H T Shen) (Rotterdam: Balkema, 1999) p. 1049
15. Andreas E L, in *The Atmospheric Boundary Layer over Polar Marine Surfaces* (CRREL Monograph 96-2) (Philadelphia: American Society for Testing and Materials, 1996) p. 38
16. Lepparanta M, in *Physics of Ice Covered Sea* Vol. 1 (Ed. M Lepparanta) (Helsinki: Helsinki University Printing House, 1994) p. 305
17. Mellor M *Mechanical Behavior of Sea Ice* (CRREL Monograph 83-1) (Philadelphia: American Society for Testing and materials, 1983)